

RESEARCH ARTICLE | SEPTEMBER 26 2024

## Aluminum relaxation as the source of excess low energy events in low threshold calorimeters

Roger K. Romani  



*J. Appl. Phys.* 136, 124502 (2024)

<https://doi.org/10.1063/5.0222654>



### Articles You May Be Interested In

Impedance Measurement of a Gamma-Ray TES Calorimeter with a Bulk Sn Absorber

*AIP Conference Proceedings* (December 2009)

Cryogenic micro-calorimeters for mass spectrometric identification of neutral molecules and molecular fragments

*J. Appl. Phys.* (September 2015)

A proton decay detector using Pb/scintillator calorimeter

*AIP Conference Proceedings* (August 2000)



Journal of Applied Physics

Special Topics Open  
for Submissions

[Learn More](#)

# Aluminum relaxation as the source of excess low energy events in low threshold calorimeters

Cite as: J. Appl. Phys. **136**, 124502 (2024); doi: [10.1063/5.0222654](https://doi.org/10.1063/5.0222654)

Submitted: 21 June 2024 · Accepted: 10 September 2024 ·

Published Online: 26 September 2024



Roger K. Romani<sup>a)</sup> 

## AFFILIATIONS

Department of Physics, University of California, Berkeley, California 94703, USA

<sup>a)</sup>Author to whom correspondence should be addressed: [rkromani@berkeley.edu](mailto:rkromani@berkeley.edu)

## ABSTRACT

A previously unexplained background called the Low Energy Excess has negatively impacted the reach of a variety of low threshold calorimeters including light dark matter direct detection and coherent elastic neutrino-nucleus scattering experiments. The relaxation of stressed aluminum films as mediated by the motion of dislocations may account for these observations.

© 2024 Author(s). All article content, except where otherwise noted, is licensed under a Creative Commons Attribution (CC BY) license (<https://creativecommons.org/licenses/by/4.0/>). <https://doi.org/10.1063/5.0222654>

## I. INTRODUCTION

Low threshold calorimeters used for rare event searches (e.g., light dark matter direct detection and coherent elastic neutrino-nucleus scattering) have observed an excess of low energy phonon events often called the Low Energy Excess (or LEE), which has constrained their science reach.<sup>1–3</sup> The rate of this background has been observed to rise around  $\sim 100$  eV, with eV scale threshold detectors observing LEE rates approaching the order of Hz. Individual LEE events have been observed to involve no ionization,<sup>4</sup> but to otherwise mimic a particle interaction in pulse shape.<sup>5</sup> Additionally, this background has been observed to decrease in rate with time since the cryogenic system has been cooled down, and to reset at least in part when the detector is warmed up and re-cooled.<sup>5</sup> Taken in concert, these observations indicate that the LEE is not a previously unknown particle background, but instead a detector specific effect. Existing models of low energy backgrounds in ionization sensitive detectors<sup>6</sup> do not explain either the rate<sup>6</sup> or the lack of ionization<sup>4</sup> of LEE events.

Recent work has shown that the relaxation of mechanical stress associated with the detector holding can create events that mimic the LEE in spectral shape and time dependence.<sup>7</sup> However, even after the detector holding stress was greatly reduced, a residual LEE component remained, which Ref. 7 attributed to the relaxation of thermally induced stress in the films from which the detector readout sensors were constructed.

In this paper, I present a model of how the relaxation of aluminum films can create events that are consistent with the LEE.

As no first-principles model of LEE events has been proposed, this model represents an important first step toward a testable model of excess events. This model specifically focuses on the relaxation of aluminum, due to its wide use in low temperature devices including TESs (Transition Edge Sensors),<sup>8</sup> KIDs (Kinetic Inductance Detectors),<sup>9</sup> and superconducting qubit-based devices.<sup>10,11</sup> Different materials with a similar structure (FCC metals with low Peierls stresses, e.g., Au and Cu) may also relax similarly. See [Appendix C](#) for further discussion.

This model may also be applicable to observations of relaxing quasiparticle burst rates in quantum circuits,<sup>12,13</sup> but focuses on “LEE” observations in calorimeters used as particle detectors.

## II. OVERVIEW

In this paper, I present a model showing that dislocation mediated relaxation in thermally stressed aluminum films produces events that are broadly consistent with the LEE (see [Fig. 1](#) for a graphical overview of this model).

- When deposited on silicon or similar substrates and when cooled to mK temperatures, differential thermal contraction between the substrate and aluminum will induce stresses on the order of 100s of MPa,<sup>14,15</sup> well in excess of the aluminum bulk yield strength.
- The stressed film will partially relax through the motion of dislocations;<sup>15</sup> however, some of these dislocations will become stuck at “pinning” sites in a metastable state.<sup>16–18</sup>

22 November 2024 20:48:59

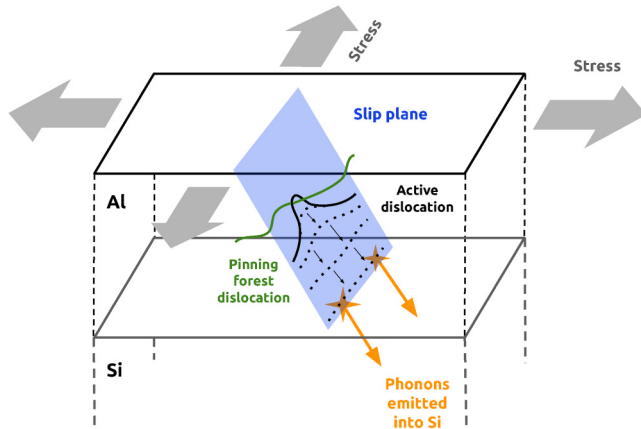


**FIG. 1.** A sketch of the model discussed in this paper. An aluminum film deposited on a silicon (or other crystal) substrate contracts relative to the substrate when cooled to mK temperatures, stressing the film. The relaxation of this film is mediated by dislocations (thick lines), which allow the film to deform through its motion. These dislocations can become stuck or “pinned” (shown here pinned against a “forest dislocation,” see the text), trapping them in a metastable state. These dislocations can tunnel free at later times and accelerate across the film. When these dislocations hit the film–substrate interface, they decelerate quickly, releasing energetic phonons into the silicon substrate.

- These metastable pinned states will later relax through tunneling.<sup>19</sup> The relaxation rate of these pinned states scales approximately as  $1/t$  for a generic model.
- Once dislocations are released from the pinned state, they will accelerate toward the film–crystal interface, where their impact with the film–crystal interface will release energy in the form of phonon bursts. These phonons are emitted in close proximity to the film–crystal interface and are primarily directed down into the crystal, leaving little energy in the film in which the relaxation took place.

To model the properties of these dislocation relaxation events, I created two codes (available publicly at Ref. 20):

- A one-dimensional numerical evaluation of the dislocation equations of motion (see Sec. V and Appendix A) to simulate the spectrum of phonons emitted from a differential length of dislocation interacting with the film–crystal interface.
- A Monte Carlo-based simulation of the spectrum expected from the relaxation of many dislocations given an average dislocation density and stress field (see Sec. VI and Appendix A). This simulation uses the results of the previous simulation to inform the efficiency of converting stress energy to above-gap phonons for a given dislocation configuration.

These codes rely on linear elasticity theory and, therefore, fail to accurately model the dynamics of dislocations moving close to the speed of sound or within several interatomic spacings of the film–crystal interface (see Sec. V). In this model, dislocations that create the LEE are common in this regime. Additionally, the Monte Carlo-based simulation neglects the role of grain boundaries, which

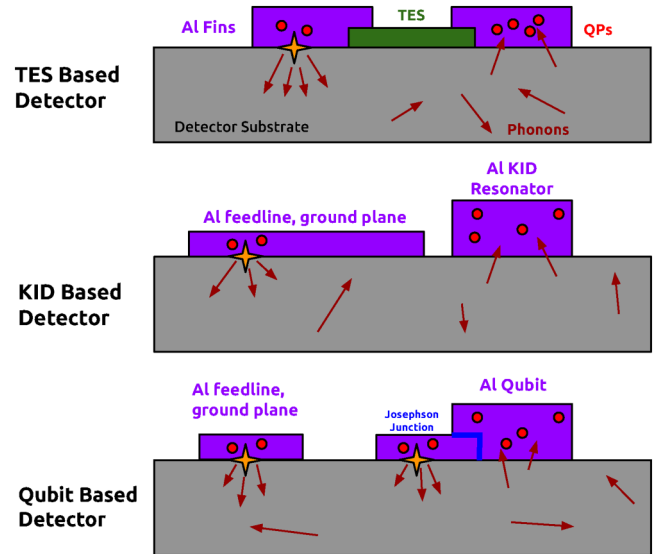


**FIG. 2.** Sketches of various low temperature detector architectures, showing the creation and sensing of LEE events caused by aluminum relaxation. In each detector type (TES, KID, qubits, e.g.,<sup>10,11</sup>), aluminum (purple) is commonly used in constructing phonon collection fins, wiring, resonators, and Josephson junctions. This model predicts that aluminum relaxation (orange stars) creates bursts of phonons (dark red) in the detector substrates, which in turn create quasiparticles (red) in the detector superconductors. Depending on the rate and energy scale, these can appear as individual events, sub-threshold noise, or a residual quasiparticle population (“quasiparticle poisoning”). Relaxation may also inject quasiparticles directly into the detector superconductors (see the text). Sketches are not to scale.

would serve to impede dislocations, changing both the depinning and phonon emission processes (see Sec. VI for further discussion). See Appendix D for a discussion of possible future work.

I will conclude by summarizing experimental evidence for this model, highlighting areas of tension between my simulations and experimental results, and by discussing the implications for low threshold cryogenic calorimeter design and operation (see Fig. 2).

### III. METAL FILM STRESS AND DEFORMATION

When thin aluminum films (used to construct, e.g., phonon collection fins or wiring in cryogenic DM detectors) are deposited on common crystalline substrates (e.g., silicon, sapphire, and germanium) and are cooled to mK temperatures, they will contract relative to the substrate by a factor of  $\epsilon \approx 4 \times 10^{-3}$ .<sup>14</sup> This biaxial strain induces a stress of  $\sigma \approx 400$  MPa, well in excess of both the  $\sim 1$ – $10$  MPa Peierls stress<sup>21</sup> (inherent to dislocation transport through the crystal lattice) and 100–200 MPa yield stresses measured in thin aluminum films.<sup>22</sup>

Metals deform through the motion of dislocations, line-like defects in the crystal structure which are driven by stress fields. To completely relax a  $\sim 4 \times 10^{-3}$  strain, dislocations at a density of  $\sim 10^{10} \text{ cm}^{-2} = (100 \text{ nm})^{-2}$  would need to travel  $\sim 100$  nm.<sup>16</sup> These scales indicate that dislocations will travel distances on the

order of the dislocation spacing and a significant fraction of the film thickness. Simulations of this process confirm these estimates and suggest that the residual stresses are on the order of 100 MPa.<sup>15</sup>

#### IV. DISLOCATION PINNING AND DEPINNING

As they travel through the metal crystal, individual dislocations may become stuck on obstacles (often called “pinning sites” or “locks”), becoming trapped in metastable excited states. Both dislocations that are not coplanar with the moving dislocation (“forest dislocations”)<sup>23</sup> and substitutional impurity atoms<sup>18</sup> are plausible candidates for these pinning sites. A detailed comparison of these two pinning mechanisms will be left for future work and will not be considered further here, where I will focus on forest dislocation pinning.

In either case, a dislocation lock will immediately fail when the resolved shear stress on the dislocation exceeds a critical stress,

$$\tau_c = \alpha \mu b / L \approx \alpha \frac{(6\text{GPa})}{L/(1\text{nm})}, \quad (1)$$

where  $\mu$  is the shear modulus,  $b$  is the Burgers vector, and  $L$  is the length of the dislocation pulling on the pinning site (longer dislocations will induce more force on a pointlike pinning site).<sup>18</sup>  $\alpha$  is a dimensionless constant ranging from  $\sim 0.8$ <sup>23</sup> in the case of certain forest dislocation locks (Lomer–Cottrell locks) to  $\sim 0.01$  in the case of certain substitutional atom pinning sites,<sup>18</sup> which quantifies the strength of the pinning.

Dislocations with an actual resolved shear stress  $\tau$  on the pinned dislocation close to the critical stress  $\tau_c$  can tunnel from the metastable pinned state into the free state at arbitrarily low temperatures. Mott<sup>19</sup> estimates the rate of this tunneling as

$$r(\tau) = v_D \exp\left(-2\mathbb{A}a\eta(\tau)\sqrt{\frac{2MW_0}{\hbar^2}}\right), \quad (2)$$

where  $\eta = (1 - \tau/\tau_c)$ ,  $v_D$  is the Debye frequency,  $\mathbb{A}$  is a constant Mott takes to be unity,  $a$  is the interatomic spacing,  $W_0$  is an activation energy which Mott takes as  $\sim 1$  eV, and  $M$  is the mass per unit width of the tunneling entity which I take as the mass of one aluminum atom (although other estimates imply it could be somewhat lower<sup>24</sup>). Using these estimates, the tunneling rate becomes

$$r(\tau) \approx v_D \exp(-900\eta(\tau)) = v_D \exp(-\Gamma\eta(\tau)). \quad (3)$$

Note that different authors give significantly different estimates of these factors, see, e.g., Refs. 24 and 25.

The total depinning rate  $R(t)$  (where  $t$  is the time after cool-down) for a large number  $N$  of pinned dislocations in a metal film can be estimated by assuming the probability distribution of  $\eta$  is flat and ranges between 0 and 1. This is equivalent to the assumption that  $\tau$  is randomly distributed from 0 to  $\tau_c$  at every pinning site, which appears reasonable given the pre-stress dislocation starting position (setting  $\tau$ ), pinned dislocation length (setting  $\tau_c$ ), and local stress field (set by, e.g., the location of close by grain boundaries) would be expected to vary quasi-randomly for each individual pinned dislocation. In reality, experiments are only sensitive to  $\eta$  in

a narrow range around  $\eta \approx 0.05$ , given the need to relax on time scales comparable to the length of an experiment. In any case, taking the “flat  $\eta$ ” approximation, I integrate over  $\eta$  to obtain

$$R(t) = N \int_0^1 r(\eta) \exp(-r(\eta)t) d\eta \quad (4)$$

$$= \frac{N}{\Gamma t} (\exp(-v_D t e^{-\Gamma}) - \exp(-v_D t)), \quad (5)$$

where the factor in parenthesis approaches one for  $\Gamma \gg \ln(v_D t)$  and  $v_D t \gg 1$ , leaving us with

$$R(t) \approx \frac{N}{\Gamma t}. \quad (6)$$

Critically, this estimate indicates that the upset rate falls off with  $1/t$  rather than exponentially. The effective measured time constant of the LEE rate will, therefore, scale with the time at which the measurement was taken (consistent with observations both in detectors<sup>5</sup> and in quantum circuits<sup>12</sup>). The  $1/t$  scaling only holds assuming that the probability distribution of  $\eta$  is relatively flat; subsequent warm up/cool-down cycles (in, e.g., Ref. 5) may alter this scaling.

Detailed atomistic simulations of the dislocation depinning process are needed to validate this model and to improve depinning rate estimates (i.e., to model  $\Gamma$ ).

#### V. PHONON CREATION

After unpinning, dislocations will accelerate through the film with essentially no friction. Both electron and phonon scattering is frozen out due to the superconductivity of the film and the low temperature, and the radiation of energy from the dislocation through interactions with the Peierls potential is generally agreed to be small.<sup>26,27</sup> Eventually, these dislocations will hit an obstacle, such as the film–substrate interface, grain boundaries, or forest dislocations. In general, the deceleration of these dislocations will be damped through the radiation of phonons.<sup>16</sup>

In this section, I will sketch a classical version of the deceleration process following Ref. 16. I will only explicitly consider dislocation interactions with the film–substrate interface, as this interface should remain essentially unchanged throughout the dislocation interaction. It is important to emphasize that this classical continuum approach undoubtedly neglects important effects, especially the damping and phonon emission from the dislocation within several  $b$  of the interface and around  $c_l$ . Better simulation of this process (possibly quantizing the phonon emission process as in Ref. 28) will be left to future work.

The force per unit length of a dislocation near the film–crystal interface can be calculated with the “image dislocation” method<sup>29</sup> as

$$F^* = \frac{dF}{dL} = \tau b + \frac{\mu_f b^2 \mu_s - \mu_f}{2\pi \mu_s + \mu_f x}, \quad (7)$$

where  $x$  is the distance between the dislocation and film–substrate interface along the slip plane,  $\mu_f$  and  $\mu_s$  are the shear moduli of the

film and substrate, respectively, and  $\tau$  is the resolved shear stress on the dislocation due to bulk stress in the film. Reference 16 gives the effective mass per unit length of the dislocation as

$$m^* = \frac{\mu_f b^2}{4\pi c_t^2} \ln\left(\frac{c_t}{\gamma\omega b}\right), \quad (8)$$

such that at every given point, the effective vibration frequency of the dislocation (and of emitted phonons) is given by Ref. 16 as

$$\omega(x) = \sqrt{\frac{dF^*}{dx}} = \frac{c_t}{x} \sqrt{2 \frac{\mu_s - \mu_f}{\mu_s + \mu_f} \ln\left(\frac{c_t}{\gamma\omega(x)b}\right)}, \quad (9)$$

where  $\gamma \approx 1.78$  and  $c_t$  is the transverse speed of sound in the film.

The damping force on a vibrating dislocation<sup>16</sup> is

$$F_{\text{rad}}^* = \frac{dF_{\text{rad}}}{dL} = \frac{\mu_f b^2 \omega}{8c_t^2} v. \quad (10)$$

In addition to this damping term, the dislocation loses energy through reductions in its effective mass  $m^*$  such that the total energy radiated into the phonon system by a differential length of dislocation is

$$\frac{\partial E_{\text{rad}}}{\partial L} = \int \left( F_{\text{rad}}^* v + \frac{1}{2} v^2 \frac{dm^*}{dt} \right) dt. \quad (11)$$

The energy radiated into above-gap phonons can be calculated by only summing energy emitted by the phonon system while  $\hbar\omega > 2\Delta_{AI}$ . In general, these phonons will cause events in detectors, given their ability to create the quasiparticles which detection techniques are sensitive to. TES-based detectors have some additional sensitivity to sub-aluminum-gap phonons, given that phonons can be directly absorbed in the TES itself.

Using these equations of motion, the deceleration of the dislocation and the properties of associated phonon radiation can be calculated numerically (see Fig. 3, Appendix A).

Imposing phonon-dislocation momentum conservation (as in Ref. 30) implies that phonons which cause the dislocation to decelerate are directed through the crystal–film interface at close range ( $\sim$ nm). Simulations show that  $\sim$ 80%–90% of the above-gap phonon energy is radiated into the crystal, with only a small fraction of above-gap energy radiated backwards into the film (see Figs. 4 and 5).

Several effects likely serve to increase the amount of energy deposited into the phonon system (vs absorbed locally in the film) compared to the behavior simulated here. First, the phonon damping given by Ref. 16 was calculated for dislocations with  $v \ll c_t$ . This linear first-order approximation of the phonon damping likely under-estimates the amount of damping the fast-moving dislocation experiences while first interacting with the interface, implying that there is more emission into the crystal than simulated here. Second, any phonon emitted into the film has a high probability of leaking energy into the crystal, either through escaping without interacting (given the  $\sim$   $\mu$ m mean free paths of

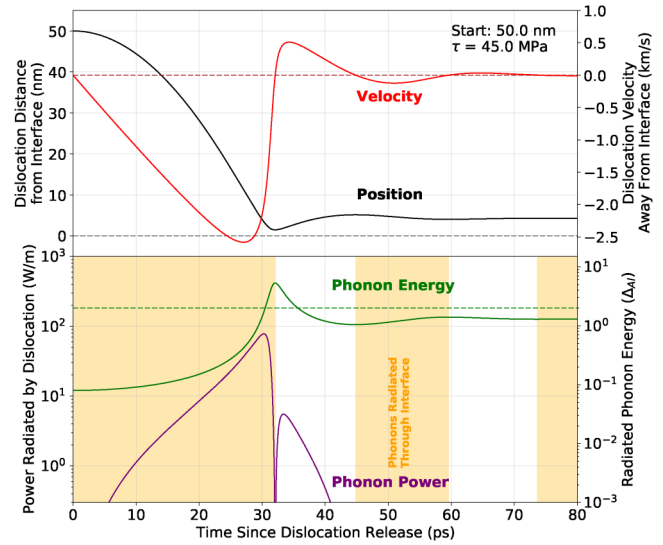


FIG. 3. The simulated motion and phonon radiation of a typical differential length of dislocation (starting 50 nm away from the film–substrate interface, in a 45 MPa resolved shear stress field). Regions where the dislocation is emitting phonons into the substrate are shaded in orange. The green dotted line is at energy  $2\Delta_{AI}$ ; phonons radiated with an energy above this line (and possibly below, see the text) will be measured by detector readout sensors.

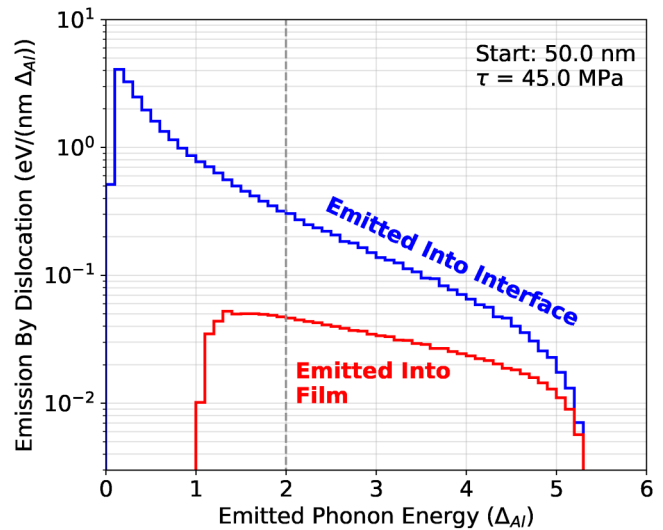
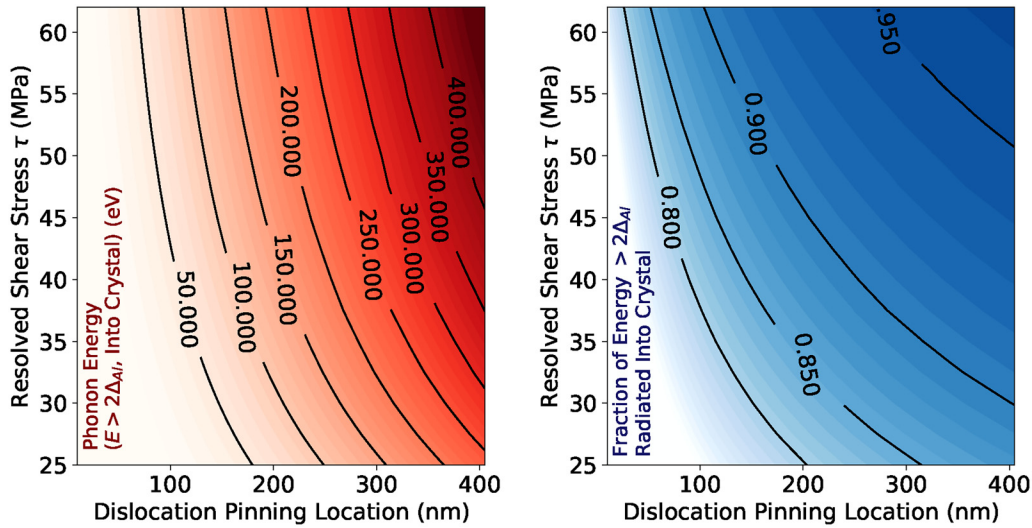


FIG. 4. The simulated spectrum of phonons emitted from the dislocation differential length shown in Fig. 3. The blue spectrum shows the spectrum of phonons emitted downward into the film–substrate interface, and red shows the spectrum of phonons emitted upwards into the film. The dotted gray line is at  $2\Delta_{AI}$ .

22 November 2024 20:48:59



**FIG. 5.** The simulated energy of above-aluminum-gap phonon energy radiated into the crystal substrate through the film–substrate interface (left), and the fraction of emitted above-aluminum-gap phonons that are directed into the interface, as opposed to into the film (right). For clarity, contours on the right plot are cut off at 0.8. Note that for initial pinning locations beyond  $\sim 65$  nm, the dislocation becomes supersonic.

close-to-gap phonons<sup>31</sup>) or through downconversion in which quasi-isotropic secondary phonons are emitted. Finally, this simulation assumes that detectors are only sensitive to above-aluminum-gap phonons, which neglects the often considerable amount of sub-gap phonon sensitivity in TES-based detectors. Vastly, more sub-gap phonons are emitted into the crystal phonon system compared to the film (see Fig. 4), meaning that detectors sensitive to these phonons are expected to see less energy absorbed locally.

Broadly, these events should appear to be approximately consistent with substrate phonon events (e.g., calibration events and DM interactions), in which all energy partitions equally between all readout channels observing the same crystal (see, e.g., Ref. 32). Due to the sub-ns time scales involved, they should also deposit energy quickly compared to the time scales of the sensor.

Improved simulations (see Appendix D) would greatly aid in more accurately modeling the dislocation deceleration and phonon emission process, and lead to more realistic estimates of the amount of energy absorbed in the film as opposed to emitted into the crystal phonon system. Quantizing the phonon emission process (using, e.g., the dislon approach<sup>25</sup>) may also be important to more accurately simulating this model. As discussed above, these improvements would be expected to bring the fraction of phonons emitted into the crystal vs the film into closer agreement with experimental data.

It is more difficult to estimate the effect of improving simulations on the reconstructed above-gap phonon energy emitted into the crystal during dislocation deceleration (and, therefore, the energy scale of relaxation events). Higher order corrections to the phonon emission process would be expected to increase the rate of deceleration close to the interface, shifting the phonon emission spectrum to higher energies. As an absolute upper bound, these

simulations indicate that around 15% of the initial stored dislocation energy is converted to above-gap phonon energy in the crystal, meaning that if dislocation energy is converted into above-gap phonons with 100% efficiency, no more than an order of magnitude shift in event energy is expected. While such a large shift seems implausible, the effects on the spectrum of events created by this process (see Fig. 6) could be compensated for by assuming that

22 November 2024 20:48:59

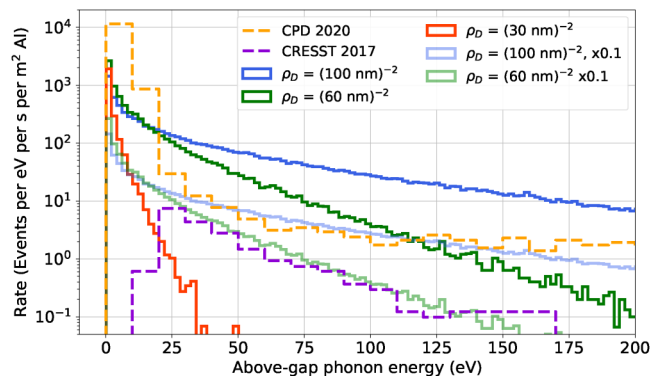


**FIG. 6.** The simulated spectrum of phonon energies for dislocation relaxation events at various dislocation densities and at a bulk stress  $\sigma_0 = 120$  MPa for a simulated detector 1 week after cooldown (see the text). Experimental measurements from Refs. 2 and 3 are superimposed. The lighter colored blue and green lines correspond to the dark blue [ $\rho_D = (100 \text{ nm})^{-2}$ ] and dark green [ $\rho_D = (60 \text{ nm})^{-2}$ ] spectrum scaled down by one order of magnitude, to account for systematic uncertainties (see the text). See Sec. VI for details on the simulation and Appendix B for details on the scaling of experimental results.

the dislocation mean free path is somewhat smaller than expected (e.g., a higher dislocation density than expected).

## VI. SPECTRUM SIMULATION

In general, the phonon energy released by a dislocation relaxation event depends on the resolved shear stress experienced by the dislocation and the distance between the dislocation pinning point and the interface.

To simulate the spectrum of energies that would be expected for dislocation relaxation events of this type, I sampled the distribution of possible dislocation resolved shear stresses and starting locations. Given a dislocation density of  $\rho_D$ , the distance that an otherwise unobstructed dislocation was pinned away from the film interface was drawn from the distribution

$$\Pr(h_{\max})_{\tau} = \rho_D L(\tau) e^{-h_{\max}/(\rho_D L(\tau))}, \quad (12)$$

where  $L(\tau)$  is the length of the pinned dislocation [see Eq. (1)]. Loosely taking the results in Ref. 15 (which were performed in two rather than three dimensions and assume a manually set dislocation source density of  $50 \mu\text{m}^{-2}$ ), I simulate three spectra for  $\rho_D = (30 \text{ nm})^{-2}$ ,  $(50 \text{ nm})^{-2}$ , and  $(100 \text{ nm})^{-2}$ . These dislocation densities are broadly consistent with the wide range of values reported in the literature (see, for example, Refs. 33, 34, and 35). I neglect the role of grain boundaries, which for small grains may shorten either the length or mean free path of dislocations.

Resolved shear stresses  $\tau$  were determined by assuming that the tensile stress  $\sigma_0$  was constant across from the film, and by sampling over the orientations of the slip plane relative to the applied tensile stress, parameterized by the azimuthal angle  $\theta$ ,

$$\Pr(\theta) = \cos(\theta), \quad (13)$$

$$\tau(\theta) = \frac{\sigma_0}{2} \sin(2\theta). \quad (14)$$

Again referencing the results of the simulation in Ref. 15, I take  $\sigma_0 = 120 \text{ MPa}$ .

After drawing values for  $h_{\max}$  and  $\tau$ , the total above-gap phonon energy emitted into the substrate  $E_{\text{tot}}$  was calculated for each simulated event (see Fig. 6).

The total number of active pinning sites was estimated by assuming that every (otherwise unimpeded) dislocation travels a distance  $d = \epsilon/(\rho_D b)$ , where  $\epsilon \approx 4 \times 10^{-3}$  is the relative strain created by differential thermal contraction, and by assuming that the mean free path for the dislocation is  $\lambda = 1/(\sqrt{\rho_D})$ .

For this depinning process, I only consider one type of lock, specifically the Lomer–Cottrell lock. I define  $\phi$  as the fraction of dislocation interactions, which will result in Lomer–Cottrell pinning, and take  $\phi = 24/144$ ,<sup>36</sup> assuming that the interacting dislocations of Burgers vectors are randomly chosen from the 144 independent Burgers vector configurations for interacting dislocations traveling on two separate slip plane on the Thompson tetrahedron.<sup>36–38</sup> Only 24 configurations will result in a Lomer–Cottrell lock,<sup>36–38</sup> the pinning site I consider in this paper. (Most of the remainder of interactions produce other types of locks, e.g.,

Hirth or Lomer locks, as well as interactions that are “glissile,” i.e., more weakly interacting.<sup>36</sup>) The fraction  $f$  of appropriately pinned dislocations is, therefore, roughly

$$f \approx 1 - e^{-d/\lambda} = 1 - \exp\left(-\frac{\epsilon\phi}{b\sqrt{\rho_D}}\right), \quad (15)$$

which gives a total event rate

$$R(t) = \frac{A_{\text{Al}}\rho_D}{\Gamma t} \left(1 - \exp\left(-\frac{\epsilon\phi}{b\sqrt{\rho_D}}\right)\right) \quad (16)$$

using Eq. (6). One week after cooldown, the total rate of events that emit non-zero amounts of above-gap energy is, therefore, around 6.0, 16.2, and 16.4 mHz/(Al mm<sup>2</sup>) for  $\rho_D = (30 \text{ nm})^{-2}$ ,  $(60 \text{ nm})^{-2}$ , and  $(100 \text{ nm})^{-2}$ , respectively.

Figure 6 shows the result of these simulations. At values of  $\rho_D$  derived from literature expectations,<sup>33–35</sup> the simulated spectral shapes broadly match experimental observations, but seem to overestimate the observed rate by about an order of magnitude. As in this model, the spectral rate is correlated to the spectral shape, choosing different values of  $\rho_D$  cannot simultaneously fit the rate and shape of the experimental spectra. I instead show that an ad-hoc scaling down of the spectra by an order of magnitude (see Fig. 6) produces better agreement with the data.

Two sources of uncertainty might explain this discrepancy between simulation and experiment. First, as discussed in Appendix B, uncertainty in the precise time at which a published spectrum was taken and the aluminum coverage of a given detector might introduce a scaling of the experimental curves by as much as a factor of two. More importantly, in this model, the total estimated spectra rate scales as

$$\frac{dR}{dE}(t) \propto \frac{1}{\Gamma} \propto \frac{1}{\mathbb{A}\sqrt{MW_0}}. \quad (17)$$

Given that  $\mathbb{A}$ ,  $M$ ,  $W_0$  were all only estimated at the  $\mathcal{O}(1)$  level by Mott,<sup>19</sup> it is easy to imagine that the true value of  $\Gamma$  might differ from my estimate by an order of magnitude, explaining the discrepancy between these simulations and previous experiments. Finally, other considerations (e.g., spatially varying dislocation densities and dislocation–grain boundary interactions) may introduce additional corrections to this model in higher fidelity simulations.

## VII. EXPERIMENTAL EVIDENCE

In addition to the well documented observation of low energy excesses in dark matter direct detection experiments, several pieces of experimental evidence support this model.

Low temperature relaxation of stressed aluminum through non-thermal processes (i.e., tunneling) is supported by the literature. Aluminum has been observed to deform below liquid helium temperatures<sup>39</sup> and over very long periods of time.<sup>40</sup> This long period deformation has been reported to occur in individual sudden relaxation events interspersed with long periods where no relaxation occurs,<sup>41</sup> possibly corresponding to individual dislocation relaxation events. In addition to these “quantum creep” type

observations, dislocation tunneling through pinning sites has been observed in “internal friction” type experiments, which have allowed for the observation of dislocation pinning and depinning well below the superconducting transition.<sup>25,34,42</sup> Work hardening type effects (i.e., pinning increasing with increasing dislocation densities) have also been observed,<sup>34</sup> strongly suggesting that dislocation–dislocation interactions play a role in governing thin film aluminum relaxation. At higher temperatures, thin aluminum films on silicon have been observed to yield under thermal stress.<sup>22</sup>

The interaction of dislocations with phonons is well established through theory and simulation (see, e.g., Refs. 28 and 43). Unfortunately, the regime described in this paper (the sudden deceleration of dislocations creating high energy phonons) does not appear to be well-studied.

### VIII. IMPLICATIONS FOR DETECTOR DESIGN

Events of these types would form both backgrounds and noise (sub-threshold) events for current generation low temperature detectors that use aluminum thin films. Reducing the rate of these excess events is, therefore, key to performing low background measurements and building detectors with good energy resolution.

Most obviously, the rate of these events could be reduced by reducing the amount of aluminum on these devices. Of course, excess non-instrumented metal films on the device surface also serve to “soak up” phonons, reducing the energy absorbed in individual sensors from phonon mediated events.

Changes to the material properties of the film could also reduce the impacts of the LEE. As suggested by Fig. 6, increasing the dislocation density (through, e.g., work hardening) may best serve to decrease the rate of high energy events. Decreasing interface grain sizes to reduce the number of dislocations that are long enough to spontaneously relax could have a similar effect. The opposite approach (annealing to decrease dislocation densities) seems likely to produce limited improvements, given the simulations shown in Fig. 6 and that dislocations will naturally be seeded during the cooldown,<sup>15</sup> effectively undoing some of the effects of annealing. Any changes to the material properties of the aluminum films would need to preserve both a good coupling to the crystal phonon system and a high quasiparticle diffusion length, potentially posing difficulties when, e.g., increasing dislocation density or decreasing interface grain sizes.

Finally, attempts could be made to artificially depin these metastable dislocations by temporarily *increasing* the stress in the aluminum films on the device surface. This could be achieved by, e.g., flexing the detector substrate (which would be impractical for thick dark matter detectors) or by compressing the films from above to increase the von Mises deviatoric stress in the film. Once the excess film stress was reduced, the films would be left in a more relaxed state, presumably with fewer dislocation relaxation events.

If eliminating relaxation events from aluminum proves difficult, substituting other materials for aluminum (see Appendix C) in low temperature calorimeters may serve to lower the rate of LEE events. Other materials used for, e.g., phonon collection fins would need to have similar superconducting transition temperatures (to retain sensitivity to similar parts of the phonon spectrum), to have good quasiparticle propagation, and efficient phonon absorption

from the substrate. Finally, detector schemes that use Josephson junctions (e.g., qubit-based detectors<sup>10,11</sup>) may struggle to completely eliminate aluminum in their designs, given the favorable properties of aluminum for constructing Josephson junctions.

### IX. TENSION WITH EXPERIMENTS

This paper aims to present a proof-of-concept model illustrating that stress relaxation in low temperature aluminum can create phonon bursts consistent with the LEE, making simplifying assumptions to more easily model the core relaxation behavior. Two areas where the model is in tension with experimental results should be explicitly noted.

First, this model predicts that ~10%–20% of phonons from a dislocation relaxation event are emitted into the film (as opposed to into the crystal). Multiple experiments including Ref. 32 have observed that events that primarily coupled to the phonon system seem to entirely couple to the phonon system. While more accurate simulation and experimental effects are likely to significantly relax this tension (see Sec. V), future experimental and phenomenological work should focus on this potential discrepancy.

Second, the simulated spectra in Fig. 6 differ in rate from the experimental results.<sup>2,3</sup> As discussed in Sec. VI, this discrepancy can be resolved by assuming a somewhat different value of  $\Gamma$  than estimated by Mott.<sup>19</sup>

### X. CONCLUSION

In this paper, I employ a model to show that the relaxation of thermal stress in aluminum films (as mediated by dislocations) can produce sudden bursts of phonons broadly consistent with the LEE. This model closely reproduces the observed rate of LEE events, the qualitative rate time dependence, the approximate spectrum of event energies, and the primary coupling to the phonon system observed for LEE events. Of course, any given experiment might host multiple types of LEE (e.g., experiments with a significant amount of dielectrics might also observe the events described in Ref. 6), meaning that this model might not fully describe LEE observations in any given experiment.

Further experiments (e.g., testing the relation between excess rates and aluminum coverage) as well as phenomenological work (e.g., atomistic modeling of dislocation depinning through tunneling, the radiation of phonons during deceleration, and the effects of realistic dislocation/grain configurations at the film–crystal interface, see Appendix D) are needed to further support or contradict this model. In light of this work, relaxation processes in other materials commonly used in low temperature detectors (e.g., tungsten, niobium, and gold) should be more fully considered, as they may be the dominant source of the current excess, or may be responsible for events observed in future experiments.

Recent interest in the links between the low energy excess and the anomalous decoherence of superconducting qubits<sup>7</sup> suggests that extensions of this model may also provide an explanation for the so-called quasiparticle poisoning.<sup>13</sup> Low energy events that are predominantly absorbed locally in films (rather than mediated through crystal phonons) would be an especially important for qubit systems.

## ACKNOWLEDGMENTS

I thank Daniel Egaña-Ugrinovic, Matt Pyle, Daniel McKinsey, Rouven Essig, Marco Costa, Michael Williams, Daniel Baxter, Noah Kurinsky, and Junwu Huang for helpful conversations. This research was supported by US Department of Energy under Grant No. DE-SC0022354 and in part by the Perimeter Institute for Theoretical Physics. Research at the Perimeter Institute is supported by the Government of Canada through the Department of Innovation, Science and Economic Development and by the Province of Ontario through the Ministry of Colleges and Universities.

## AUTHOR DECLARATIONS

## Conflict of Interest

The authors have no conflicts to disclose.

## Author Contributions

**Roger K. Romani:** Conceptualization (equal); Data curation (equal); Formal analysis (equal); Investigation (equal); Methodology (equal); Visualization (equal); Writing – original draft (equal).

## DATA AVAILABILITY

The data that support the findings of this study are available from the corresponding author upon reasonable request. The simulation software used in this study is available publicly.<sup>20</sup>

## APPENDIX A: DISLOCATION MOTION NUMERICAL SIMULATION

As described in the overview, this paper relies on two simple Python-based simulations.<sup>20</sup>

## a. Dislocation motion and phonon radiation simulation

To simulate the motion and phonon radiation from a short length  $dL$  of dislocation impacting the film–crystal interface, the following analytic equations of dislocation motion (also described in Sec. V) were numerically solved using SciPy’s “solve\_ivp” method. Following Refs. 16 and 29, I set

$$\omega(x) = \frac{c_t}{\gamma b} \exp\left(\frac{1}{2} W\left(-4\gamma^2 \frac{\mu_s - \mu_f b^2}{\mu_s + \mu_f x^2}\right)\right), \quad (\text{A1})$$

$$m^*(x) = \frac{dm}{dL}(x) = \frac{\mu_f b^2}{4\pi c_t^2} \ln\left(\frac{c_t}{\gamma b \omega(x)}\right), \quad (\text{A2})$$

$$F_{\text{rad}}^*(x, v) = \frac{dF_{\text{rad}}}{dL}(x, v) = -\frac{\mu_f b^2 v \omega(x)}{8c_t^2}, \quad (\text{A3})$$

$$F_{\text{interface}}^*(x) = \frac{dF_{\text{interface}}}{dL}(x) = \frac{\mu_f b^2 \mu_s - \mu_f}{4\pi \mu_s + \mu_f x}, \quad (\text{A4})$$

$$F_{\text{tot}}^*(x, v) = F_{\text{rad}}^*(x, v) + F_{\text{interface}}^*(x) + \tau b, \quad (\text{A5})$$

$$\frac{dx^2}{dt^2} = \frac{F_{\text{tot}}^*(x, v)}{m^*(x)}, \quad (\text{A6})$$

where  $W$  is the Lambert  $W$  function and other symbols are defined in the main text. The initial conditions were  $x(0) = h$  and  $dx/dt(0) = 0$ , and I took  $b = 0.286$  nm,  $c_t = 3040$  m/s,  $\mu_f = 25$  GPa, and  $\mu_s = 51$  GPa.

By numerically solving these differential equations,  $x(t)$ ,  $v(t)$ ,  $\omega(t)$ ,  $\dots$  were obtained (see Fig. 3). The power radiated into phonons by a unit length of dislocation at each moment in time could also be computed using

$$P_{\text{rad}}^*(t) = F_{\text{rad}}^*(t)v(t) - \frac{1}{2} \frac{dm}{dt}(t)v^2(t), \quad (\text{A7})$$

assuming that the reduction in effective dislocation mass occurs through the radiation of phonons as described in the main text and discussed below.

During the deceleration process, phonons will be emitted in one of two directions: either into the crystal through the crystal–film interface (when the dislocation is damped while moving toward the interface, i.e.,  $F_{\text{rad}}^* > 0$ , i.e.,  $v < 0$ ) or into the film (when the dislocation is damped while moving away from the interface, i.e.,  $F_{\text{rad}}^* < 0$ , i.e.,  $v > 0$ ). The total amount of energy radiated in each direction can be computed by summing

$$\frac{dE_{\text{crystal}}}{dL} = E_{\text{crystal}}^* = \sum_{v(t) < 0} P_{\text{rad}}^*(t)\Delta t, \quad (\text{A8})$$

$$\frac{dE_{\text{film}}}{dL} = E_{\text{film}}^* = \sum_{v(t) > 0} P_{\text{rad}}^*(t)\Delta t, \quad (\text{A9})$$

where  $\Delta t$  is the time step of the simulation. Similarly, the energy of phonons emitted at a given time (and, therefore, the spectrum of emitted phonons) can be calculated using  $E_{\text{phonon}}(t) = \hbar\omega(t)$ , with the sign of  $v(t)$  used to determine if these phonons are emitted into the film or crystal. From this relation, the energy of, e.g., above-superconducting-gap phonons emitted into the crystal can be calculated using

$$E_{\text{crystal, above-gap}}^* = \sum_{v(t) < 0, \hbar\omega(t) > 2\Delta_{Al}} P_{\text{rad}}^*(t)\Delta t, \quad (\text{A10})$$

where  $\Delta_{Al}$  is the superconducting bandgap energy.

By numerically solving this differential equation and performing the above sums,  $E^*(h, \tau)$  can be simulated for a grid of realistic  $h$ ,  $\tau$  points.

As noted in the main text, this approach is only a one-dimensional analytic approximation of the true dynamics of the system. See Appendix D for more details on how these simulations could be more realistically performed in future work.

Two caveats of this approach warrant explicit recognition. First, as modeled in Sec. V, the dislocation effective mass changes as a function of position above the interface. While decreases in the

dislocation kinetic energy through a decrease in effective mass are easily interpreted as the radiation of kinetic energy through the emission of phonons, *increases* in kinetic energy due to an increase in mass are more difficult to interpret.

Second, no “elastorelativistic” corrections are applied in this model, meaning that the dislocation can accelerate beyond  $c_l$  for high stresses and large initial distances between the dislocation and interface. While this system is somewhat unique in that, e.g., dislocation–phonon damping is highly suppressed, and while supersonic dislocation motion has been experimentally observed,<sup>44</sup> supersonic dislocations remain controversial. Future work should attempt to more accurately model the motion of the dislocation close to  $c_l$ .

### b. Monte Carlo-based spectrum simulation

After simulating the emitted phonon energy per unit length of dislocation  $E^*(h, \tau)$ , I calculated the total energy emitted by the entire dislocation by integrating

$$E_{\text{tot}} = \int_y E^*(h(y), \tau) dy \quad (\text{A11})$$

$$= \int_0^{h_{\text{max}}} E^*(h(y), \tau) \frac{dy}{dh} dh. \quad (\text{A12})$$

In general, the shape  $h(y)$  of the pinned dislocation is governed by self-interaction and interactions with the pinning site, shear stress field, and the interface, leading to a complex shape likely only determinable using simulation (see Appendix D). Here, I make the assumption that the dislocation shape is linear between the pinning site and the interface, meaning that for a dislocation with total width  $L(\tau)$  [see Eq. (1)],

$$\frac{dh}{dy} = \frac{h_{\text{max}}}{L(\tau)}. \quad (\text{A13})$$

Using this assumption and the simulated  $E^*$ ,  $E_{\text{tot}}(h_{\text{max}}, \tau)$  can be calculated, as shown in Fig. 5.

Changes to this model of the initial dislocation shape  $h(x)$  (e.g., assuming that the dislocation ends are pinned away from the interface, rather than at the interface) may increase the fraction of event energy emitted into the crystal phonon system, potentially resolving some of the tension discussed in Sec. V.

This calculation yields a total energy  $E_{\text{tot}}(h_{\text{max}}, \tau)$  of, e.g., phonons emitted into the crystal above the aluminum superconducting bandgap for a given resolved shear stress  $\tau$  and pinning distance  $h_{\text{max}}$ . Using a Monte Carlo method, these were used to simulate a spectrum of events expected in a given device (see Sec. VI).  $h_{\text{max}}$  and  $\tau$  were drawn from

$$\text{Pr}(h_{\text{max}})_\tau = \rho_D L(\tau) e^{-h_{\text{max}}/(\rho_D L(\tau))}, \quad (\text{A14})$$

$$\text{Pr}(\theta) = \cos(\theta), \quad (\text{A15})$$

$$\tau(\theta) = \frac{\sigma_0}{2} \sin(2\theta), \quad (\text{A16})$$

assuming  $\sigma_0 = 120$  MPa, and for a variety of realistic  $\rho_D$  (see Sec. VI). From these drawn values,  $E_{\text{tot}}(h_{\text{max}}, \tau)$  was calculated and converted into a spectrum (see Fig. 6). These spectra were scaled assuming a total rate of events given by Eq. (6) (see Sec. VI).

## APPENDIX B: SCALING DETECTOR SPECTRA

Comparing simulated results to real data requires scaling to allow for an equal-footed test. In this appendix, I describe how the data in Refs. 2 and 3 (with data taken from the public repository described in Ref. 1) were scaled for Fig. 6. In general, the necessary information (particularly how long the detector was cold when the measurement was performed and the amount of aluminum film on the device surface) is not published, requiring some parameters to be estimated. Better understanding of these parameters may resolve some of the tension between simulation and experimental results seen in Fig. 6.

For the CRESST-III main detector described in Ref. 2, the detector was assumed to have been cold for 1 year, and the aluminum fins were assumed to be the same size as the aluminum fins for the CRESST-III light detector (LD).<sup>45</sup>

For the CPD detector in Ref. 3, the detector was assumed to have been cold for 6 weeks, and to have 2% of its 45.6 cm<sup>2</sup> surface area covered by aluminum.<sup>46</sup>

To compensate for the amount of time detectors were cold, the spectra given in Ref. 1 were scaled up by a factor of (Time Cold)/(1 Week).

## APPENDIX C: OTHER MATERIALS

This model relies upon free (unpinned) dislocations being able to easily move around in the crystal lattice under thermally induced stresses, i.e., that the Peierls stress is low compared to the thermally induced stress. In the case of aluminum, this assumption holds (see Sec. III).

Copper, gold, and other FCC metals commonly used in low temperature devices have similarly low Peierls stresses and might, therefore, create phonon bursts similar to those created by aluminum when relaxing at low temperatures. Key differences between these materials and aluminum include the effective dislocation mass and the Debye frequency (which would affect the depinning rate), as well as the speed of sound, Burgers vector length, and shear modulus (which affects the phonon emission process). The strength of dislocation pinning to either impurities or forest dislocations would also be expected to vary, which would in turn affect the depinning rate and the scale of depinned dislocations. Finally, typical dislocation densities in these materials may differ from those assumed here for aluminum. The extension of this model to other materials is left for future work. BCC metals with somewhat low Peierls stresses such as niobium<sup>47</sup> may also behave similarly to aluminum.

Materials with higher Peierls stresses such as tungsten would not be expected to deform through the mechanisms described in this paper, as their Peierls stresses greatly exceed thermally induced stresses,<sup>47</sup> making dislocation motion through the crystal lattice difficult. While these materials might yield after thermal stressing (through, e.g., cracking or interface delamination, see Ref. 48 for the delamination of W on Si), they would not be expected to

deform through the motion of dislocations as described in this model. Experimentally, thin-film tungsten has been deposited with stresses varying by several GPa (see, e.g., Refs. 49 and 50), suggesting that thermally induced 100 MPa-scale stress changes are not likely to cause macroscopic yielding (as has been observed for aluminum<sup>22</sup>).

#### APPENDIX D: FUTURE WORK

The model presented in this work could be improved by applying more existing simulation codes. In this section, I suggest areas for future improvement, ordered similarly to the sections in the main body of this paper.

Detailed predictions of the tunneling rate (that go beyond the simple estimates of Mott<sup>19</sup> used in this work) would need to rely on more accurate knowledge of the dislocation–dislocation interaction potential (assuming that these pinning sites are responsible for observations). This could be calculated as a function of resolved stress, dislocation–dislocation orientation, and dislocation distance using a density functional theory-based package such as VASP,<sup>51</sup> similar to the work done for impurity pinning sites.<sup>18</sup> Once these potentials are known, tunneling rates for each configuration could be calculated.

To more accurately calculate the energy emitted by a relaxation event, a number of additional pieces of information are needed. First, knowledge of the distribution of grain sizes at the crystal–film interface is needed. Likely, this will be provided both from characterization of real films (using, e.g., Transmission Electron Microscopy) but also simulations of film deposition (see, e.g., Refs. 52 and 53).

From this knowledge of the structure of the film, the dislocation seeding and stressing process during cooldown can be simulated in three dimensions. This should likely be undertaken with a discrete dislocation dynamics package such as ParaDIS,<sup>54</sup> which would include, e.g., boundary conditions that reflect thin films and realistic grain sizes. This simulation would inform

- The density and stress distribution of locked dislocations;
- The shape of the pinned dislocation (which informs the amount of stored energy and the speed of the unpinned dislocation when impacting the interface);
- The length of the dislocation that will impact the film–crystal interface (rather than a grain boundary).

Course grained atomistic approaches (see Ref. 55) could also be employed. The involvement of experts would of course be the key to selecting the most appropriate simulation technique.

Finally, the phonon-radiating dislocation impact at the film–crystal interface could be more accurately simulated using existing codes. Although simulations of dislocation–phonon interactions based on a course grained atomistic approach have been performed (see, e.g., Ref. 56), no existing tools seem to be designed to simulate the radiation of high energy phonons by decelerating dislocations. Some combination of existing codes and extensions based on the theory of dislocation–phonon interactions (perhaps using the “dislon” approach<sup>28</sup>) should be employed to more accurately simulate the spectrum and direction of phonons radiated during this deceleration process. This simulation could also be applied to the

impact of dislocations on, e.g., grain boundaries or forest dislocations. Impacts with grain boundaries or forest dislocations are very difficult to imagine understanding analytically and could give insight into a range of local effects (as described in, e.g., Ref. 32).

This three-dimensional simulation of phonon-radiation would start with the dislocation in a just-unpinned state, track its acceleration toward the grain boundary under the resolved shear stress field (naturally including “elastorelativistic” effects), and simulate the radiation of phonons from the dislocation as it decelerates at the interface. From this, a spectrum of emitted phonons for a given relaxation event could be calculated. Combined with knowledge of the film configuration near the interface, this could be used to create a Monte Carlo type simulation to generate spectra, which could be compared to LEE spectra measured in real detectors.

#### REFERENCES

- <sup>1</sup>P. Adari *et al.*, “EXCESS workshop: Descriptions of rising low-energy spectra,” *SciPost Phys. Proc.* **9**, 001 (2022).
- <sup>2</sup>F. Petricca *et al.*, “First results on low-mass dark matter from the CRESST-III experiment,” *J. Phys.: Conf. Ser.* **1342**, 012076 (2020).
- <sup>3</sup>I. Alkhatib *et al.*, “Light dark matter search with a high-resolution athermal phonon detector operated above ground,” *Phys. Rev. Lett.* **127**, 061801 (2021). Collaboration SuperCDMS Collaboration.
- <sup>4</sup>E. Armengaud *et al.*, “Constraints on low-mass WIMPs from the EDELWEISS-III dark matter search,” *J. Cosmol. Astropart. Phys.* **2016**, 019 (2016).
- <sup>5</sup>G. Angloher *et al.*, “Latest observations on the low energy excess in CRESST-III,” [arXiv:2207.09375](https://arxiv.org/abs/2207.09375) (2022).
- <sup>6</sup>P. Du, D. Egana-Ugrinovic, R. Essig, and M. Sholapurkar, “Sources of low-energy events in low-threshold dark-matter and neutrino detectors,” *Phys. Rev. X* **12**, 011009 (2022).
- <sup>7</sup>R. Anthony-Petersen *et al.*, “A stress induced source of phonon bursts and quasiparticle poisoning,” [arXiv:2208.02790](https://arxiv.org/abs/2208.02790) (2022).
- <sup>8</sup>K. D. Irwin, S. W. Nam, B. Cabrera, B. Chugg, and B. A. Young, “A quasiparticle-trap-assisted transition-edge sensor for phonon-mediated particle detection,” *Rev. Sci. Instrum.* **66**, 5322 (1995).
- <sup>9</sup>P. K. Day, H. G. LeDuc, B. A. Mazin, A. Vayonakis, and J. Zmuidzinas, “A broadband superconducting detector suitable for use in large arrays,” *Nature* **425**, 817–821 (2003).
- <sup>10</sup>M. D. Shaw, J. Bueno, P. Day, C. M. Bradford, and P. M. Echternach, “Quantum capacitance detector: A pair-breaking radiation detector based on the single Cooper-pair box,” *Phys. Rev. B* **79**, 144511 (2009).
- <sup>11</sup>C. W. Fink, C. P. Salemi, B. A. Young, D. I. Schuster, and N. A. Kurinsky, “The superconducting quasiparticle-amplifying transmon: A qubit-based sensor for meV scale phonons and single THz photons” (2023).
- <sup>12</sup>E. T. Mannila, P. Samuelsson, S. Simbierowicz, J. T. Peltonen, V. Vesterinen, L. Gronberg, J. Hassel, V. F. Maisi, and J. P. Pekola, “A superconductor free of quasiparticles for seconds,” *Nat. Phys.* **18**, 145 (2022).
- <sup>13</sup>K. Serniak, M. Hays, G. de Lange, S. Diamond, S. Shankar, L. Burkhart, L. Frunzio, M. Houzet, and M. Devoret, “Hot nonequilibrium quasiparticles in transmon qubits,” *Phys. Rev. Lett.* **121**, 157701 (2018).
- <sup>14</sup>J. Ekin, *Experimental Techniques for Low-Temperature Measurements: Cryostat Design, Material Properties and Superconductor Critical-Current Testing* (Oxford University Press, 2006).
- <sup>15</sup>H. Fan, Z. Li, M. Huang, and X. Zhang, “Thickness effects in polycrystalline thin films: Surface constraint versus interior constraint,” *Int. J. Solids Struct.* **48**, 1754–1766 (2011).
- <sup>16</sup>P. M. Anderson, J. P. Hirth, and J. Lothe, *Theory of Dislocations*, 3rd ed. (Cambridge University Press, Cambridge, 2017).

- <sup>17</sup>F. Nabarro, "Work hardening and dynamical recovery of F.C.C. metals in multiple glide," *Acta Metall.* **37**, 1521 (1989).
- <sup>18</sup>S. Patinet and L. Proville, "Dislocation pinning by substitutional impurities in an atomic-scale model for Al(Mg) solid solutions," *Philos. Mag.* **91**, 1581 (2011).
- <sup>19</sup>N. Mott, "LVII. Creep in metal crystals at very low temperatures," *Philos. Mag.* **1**, 568 (1956).
- <sup>20</sup>R. K. Romani, "Dislocation Relaxation Simulation for Low Energy Excess Events (DRSLEEE)," GitHub repository, <https://github.com/rkromani/LEE-Dislocation-Simulations/tree/main>
- <sup>21</sup>I. Shin and E. A. Carter, "Possible origin of the discrepancy in Peierls stresses of fcc metals: First-principles simulations of dislocation mobility in aluminum," *Phys. Rev. B* **88**, 064106 (2013).
- <sup>22</sup>J.-H. Jou and C.-S. Chung, "Mechanical characteristics of aluminum thin films on silicon and gallium arsenide," *Thin Solid Films* **235**, 149–155 (1993).
- <sup>23</sup>D. Rodney and R. Phillips, "Structure and strength of dislocation junctions: An atomic level analysis," *Phys. Rev. Lett.* **82**, 1704 (1999).
- <sup>24</sup>T. Vegge, J. P. Sethna, S.-A. Cheong, K. W. Jacobsen, C. R. Myers, and D. C. Ralph, "Calculation of quantum tunneling for a spatially extended defect: The dislocation kink in copper has a low effective mass," *Phys. Rev. Lett.* **86**, 1546 (2001).
- <sup>25</sup>T. Kosugi, D. McKay, and A. Granato, "Theory of dislocation tunneling through a pinning point," *J. Alloys Compd.* **310**, 111–114 (2000).
- <sup>26</sup>V. A. Al'shitz and V. L. Indenbom, "Dynamic dragging of dislocations," *Sov. Phys. Usp.* **18**, 1–20 (1975).
- <sup>27</sup>Y. Tang, "Uncovering the inertia of dislocation motion and negative mechanical response in crystals," *Sci. Rep.* **8**, 140 (2018).
- <sup>28</sup>M. Li, Y. Tsurimaki, Q. Meng, N. Andrejevic, Y. Zhu, G. D. Mahan, and G. Chen, "Theory of electron-phonon-dislon interacting system—Toward a quantized theory of dislocations," *New J. Phys.* **20**, 023010 (2018).
- <sup>29</sup>M. Öveçoğlu, M. Doerner, and W. Nix, "Elastic interactions of screw dislocations in thin films on substrates," *Acta Metall.* **35**, 2947–2957 (1987).
- <sup>30</sup>C. S. Coffey, "Phonon generation and energy localization by moving edge dislocations," *Phys. Rev. B* **24**, 6984–6990 (1981).
- <sup>31</sup>J. M. Martinis, "Saving superconducting quantum processors from decay and correlated errors generated by gamma and cosmic rays," *npj Q. Inform.* **7**, 90 (2021).
- <sup>32</sup>G. Angloher *et al.*, "Double TES detectors to investigate the CRESST low energy background: Results from above-ground prototypes," [arXiv:2404.02607](https://arxiv.org/abs/2404.02607) (2024).
- <sup>33</sup>S. H. Oh, M. Legros, D. Kiener, and G. Dehm, "In situ observation of dislocation nucleation and escape in a submicrometre aluminium single crystal," *Nat. Mater.* **8**, 95–100 (2009).
- <sup>34</sup>X. Liu, E. Thompson, B. E. White, and R. O. Pohl, "Low-temperature internal friction in metal films and in plastically deformed bulk aluminum," *Phys. Rev. B* **59**, 11767–11776 (1999).
- <sup>35</sup>C.-L. Liang, S.-W. Lee, and K.-L. Lin, "The mechanism of an increase in electrical resistance in Al thin film induced by current stressing," *Thin Solid Films* **636**, 164–170 (2017).
- <sup>36</sup>P. Franciosi and A. Zaoui, "Multislip in f.c.c. crystals: A theoretical approach compared with experimental data," *Acta Metall.* **30**, 1627–1637 (1982).
- <sup>37</sup>G. Saada and P. Veyssi re, "Chapter 61 work hardening of face centred cubic crystals. Dislocations intersection and cross slip," in *Dislocations in Solids* (Elsevier, 2002), pp. 413–458.
- <sup>38</sup>D. Hull and D. J. Bacon, in *Introduction to Dislocations* (Elsevier, 2011), pp. 1–20.
- <sup>39</sup>V. A. Koval, "Creep of aluminum in the temperature range 1.4–4.2 K," *Sov. Phys.: Solid State* **12**, 2347 (1971).
- <sup>40</sup>L. C. McDonald, "Creep of pure aluminum at cryogenic temperatures," Masters thesis (Texas A&M University, 1989).
- <sup>41</sup>V. A. Koval and V. P. Soldatov, "Jumplike deformation of copper and aluminum during low-temperature creep," in *Advances in Cryogenic Engineering Materials: Volume 26*, edited by A. F. Clark and R. P. Reed (Springer US, Boston, MA, 1980), pp. 86–90.
- <sup>42</sup>T. Kosugi, D. McKay, and A. V. Granato, "Measurement of dislocation tunneling through a pinning atom," *J. Phys. IV* **6**, C8 (1996).
- <sup>43</sup>Y. Cheng, M. Nomura, S. Volz, and S. Xiong, "Phonon–dislocation interaction and its impact on thermal conductivity," *J. Appl. Phys.* **130**, 040902 (2021).
- <sup>44</sup>K. Katagiri *et al.*, "Transonic dislocation propagation in diamond," [arXiv:2303.04370](https://arxiv.org/abs/2303.04370) (2023).
- <sup>45</sup>R. Strauss *et al.*, "A prototype detector for the CRESST III low-mass dark matter search," *Nucl. Instrum. Methods Phys. Res., Sect. A* **845**, 414–417 (2017).
- <sup>46</sup>C. W. Fink S. L. Watkins *et al.*, "Performance of a large area photon detector for rare event search applications," *Appl. Phys. Lett.* **118**, 022601 (2021).
- <sup>47</sup>J. C. F. Millett, M. Cotton, N. K. Bourne, N. T. Park, and G. Whiteman, "The behaviour of niobium and molybdenum during uni-axial strain loading," *J. Appl. Phys.* **115**, 073506 (2014).
- <sup>48</sup>L. Shen and Z. Chen, "A multi-scale simulation of tungsten film delamination from silicon substrate," *Int. J. Solids Struct.* **42**, 5036–5056 (2005).
- <sup>49</sup>Y. G. Shen, Y. W. Mai, Q. C. Zhang, D. R. McKenzie, W. D. McFall, and W. E. McBride, "Residual stress, microstructure, and structure of tungsten thin films deposited by magnetron sputtering," *J. Appl. Phys.* **87**, 177–187 (2000).
- <sup>50</sup>T. J. Vink, W. Walrave, J. L. C. Daams, A. G. Dirks, M. A. J. Somers, and K. J. A. van den Aker, "Stress, strain, and microstructure in thin tungsten films deposited by dc magnetron sputtering," *J. Appl. Phys.* **74**, 988–995 (1993).
- <sup>51</sup>G. Kresse and J. Furthm ller, "Efficient iterative schemes for ab initio total-energy calculations using a plane-wave basis set," *Phys. Rev. B* **54**, 11169 (1996).
- <sup>52</sup>J. Zhang and J. B. Adams, "Modeling and visualization of polycrystalline thin film growth," *Comput. Mater. Sci.* **31**, 317–328 (2004).
- <sup>53</sup>P. Smereka, X. Li, G. Russo, and D. Srolovitz, "Simulation of faceted film growth in three dimensions: Microstructure, morphology and texture," *Acta Mater.* **53**, 1191–1204 (2005).
- <sup>54</sup>M. Tang, G. Hommes, S. Aubry, and A. Arsenlis, "*ParaDis-FEM dislocation dynamics simulation code primer*" LLNL Technical Report No. LLNL-TR-501662, Lawrence Livermore National Lab., Livermore, CA, United States, 2011.
- <sup>55</sup>L. Xiong, G. Tucker, D. L. McDowell, and Y. Chen, "Coarse-grained atomistic simulation of dislocations," *J. Mech. Phys. Solids* **59**, 160–177 (2011).
- <sup>56</sup>X. Chen, L. Xiong, D. L. McDowell, and Y. Chen, "Effects of phonons on mobility of dislocations and dislocation arrays," *Scr. Mater.* **137**, 22–26 (2017).